Pure Appl. Geophys. 179 (2022), 833–844

https://doi.org/10.1007/s00024-021-02931-8

Pure and Applied Geophysics

# Clouds Affecting Total Ozone Column Measurements

A. A. Silva[1]

*Abstract*—Total ozone column (TOC) measurements have been made remotely all over the globe using ground-based and satellite probing. Other atmospheric constituents such as clouds and aerosols can interfere significantly in such measurements. In this work, the influence of clouds on TOC ground-based measurements in a tropical site is investigated using 16 months of spectral direct Sun measurements from an ultraviolet narrow-band radiometer. The results show that, on average, TOC measurements through clouds blocking the Sun ($TOC_C$) can be 0.9% (ranging from −4.6 to 3.4%) larger than TOC measurements under cloud-free skies ($TOC_{CFS}$), and TOC measurements under all-sky conditions without clouds blocking the Sun can be 0.3% (ranging from −5.4 to 2.2%) larger than $TOC_{CFS}$. In addition, the variability rate (Dobson units/min) in $TOC_C$ can be over five times that for $TOC_{CFS}$ on average.

**Keywords:** Ozone, clouds, aerosols, ultraviolet radiation.

## 1. Introduction

Solar radiation interacts with the Earth's atmosphere through scattering and absorption. Ultraviolet (UV) radiation is of particular concern here. Ozone molecules in the stratosphere (the ozone layer) are formed by solar UV wavelengths < 280 nm. The ozone layer absorbs harmful longer UV wavelengths (< 315 nm), reducing their incidence on the ground (Lautenschlager et al., 2007; Whitten & Prasad, 1985).

Ozone is a trace gas in the terrestrial atmosphere, and its atmospheric columnar amount is given by the total ozone column (TOC), which has been measured remotely using ground-based and satellite probing (Whitten & Prasad, 1985). The most precise ground-based instruments produce TOC measurement with uncertainties < 2%, while similar uncertainties are found from satellite probing (McPeters et al., 2008; Silva & Tomaz, 2012; Silva, 2007, 2013a). Although satellites can fly over the whole Earth every day, their data are validated using ground-based equipment. Naturally, owing to its fundamental importance to both the biosphere and the atmosphere, ozone remains a matter of utmost interest (Bais et al., 2015).

Clouds and aerosols are other important constituents in the atmosphere. Clouds are the most important atmospheric modulator of ground incidence of solar radiation (Calbó et al., 2005; Silva, 2011). In addition, they interfere in TOC measurements. In general, clouds can be described as a cluster of droplets formed by water vapour condensed upon a tiny aerosol particle called the condensation nucleus. However, there is no broadly accepted consensus on what the exact number of such droplets gathered together should be to be considered a cloud, especially because an aerosol plume, although not usually composed of spherical particles like cloud droplets, can fit such a description perfectly (Chiu et al., 2009; Koren et al., 2007). Furthermore, cloud detection also depends on the radiation wavelength used.

The most well-known and perhaps frequent effect of clouds on solar radiation is attenuation (Calbó et al., 2005). However, some cloud genera are also closely related to the so-called radiation enhancement event (REE), in which there is a sudden increase in the flux of radiation towards the ground from radiation scattered from the thinner parts of clouds (Parisi & Dows, 2004; Silva et al., 2019; Silva, 2013b). Fundamentally, there exist three main mechanisms capable of yielding REEs:

i. The Sun disk is not obscured by a cloud while its diffuse component is increased through forward scattering on the sides of vertically developed

[1] Instituto de Estudos Avançados (IEAv), Trevo Cel Av José Alberto Albano do Amarante 1, Putim, São José dos Campos, SP CEP 12228-001, Brazil. E-mail: silvalluv@gmail.com

clouds, enhancing the global radiation on the ground.

ii. The Sun disk is obscured by a thin-layered cloud or by the borders or thin parts of clouds, reducing the Sun's direct beam, but the diffuse component is increased through forward scattering that more than compensates the reduction in the direct component, resulting in the enhancement of the global radiation on the ground.

iii. Snow reflects the solar radiation to the atmosphere that (including clouds and aerosols) reflects the radiation back, enhancing the downwelling component of global radiation. Similarly, an extensive cloud layer reproduces this effect in relation to mountain peaks above such a layer.

Items (i) and (ii) are feasible for the tropical site considered here.

In this study, 16 months of ground-based TOC measurements from direct Sun (DS) spectral measurements using an ultraviolet narrow-band radiometer are presented for an urban, tropical site in Brazil. Sky images are gathered simultaneously by an imager, providing images of the sky during measurements. The effects from clouds on such measurements are determined.

## 2. Site, Instruments, and Methods

### 2.1. Site Description

Belo Horizonte (BH, 19.92° S, 43.94° W, 858 m a.s.l., 331 km$^2$, 7167 inhabitants/km$^2$ in 2010, Brazil) (IBGE, 2021) is the main city in the third largest Brazilian metropolitan area. As a municipality, it has over two million vehicles outfitted with catalytic converter devices and electronic injection engines. The predominant economic activities in the area are trade, industry, and mining. Settled in a hilly area of southeastern Brazil, the city features a tropical climate of altitude (milder weather due to the area's altitude) between the savanna (Cerrado) and the remains of the Atlantic Forest (Mata Atlântica). A dry period develops from May to September, and a rainy one from November to March. Large amounts of smoke from biomass burning are blown into the area during dry periods, reinforcing the trend towards a dry scenario, where occasionally humidity can drop to around 10% during winter (June, July, and August) and early spring (September, October, and November).

### 2.2. Instruments

#### 2.2.1 The Ultraviolet Rotating Shadowband Radiometer 4

The Ultraviolet Rotating Shadowband Radiometer 4 (UVMFR4, Yankee Environmental Systems, Inc., Turners Falls, MA, USA) (Harrison et al., 1994) is the ultraviolet narrow-band radiometer used in this work. It measures spectral irradiance of global ($UV_G$) and diffuse ($UV_{Dif}$) UV radiation at centre wavelengths of 300, 305.3, 311.5, and 317.5 nm with bandwidth of 2.3–2.4 nm full width at half maximum (FWHM) through filters. The direct component of the spectral solar UV radiation ($UV_{Dir}$, which can also be represented by DS) is calculated through

$$UV_{Dir} = \frac{UV_G - UV_{Dif}}{\cos(SZA)}, \quad (1)$$

where SZA stands for solar zenith angle, and the division by the cosine reminds us that the radiometer's measurement is the cosine projection of the direct component of the solar radiation through the SZA, as the radiometer is in the flat horizontal position.

The instrument uses a semicircular metallic strip to obstruct the direct incidence of solar radiation in its sensor. For this, firstly, the strip is set in the home position by a stepper motor, allowing the measurement of $UV_G$. Secondly, the strip is rotated to a central position, blocking the sensor from $UV_{Dir}$ and allowing the measurement of $UV_{Dif}$. As a result, $\approx 3.3°$ of the sky is obstructed by the strip in addition to the solar disk. To compensate for the radiation lost from that part of the sky, another two measurements are made with the strip rotated 9° to the left and to the right off the central position. The difference between $UV_G$ and the average between the two displaced-strip measurements represents the amount of diffuse radiation blocked from the sky by the strip. That amount is added to the original measurement of $UV_{Dif}$ as a correction. The cycle of

four measurements ($UV_G$, $UV_{Dif}$, and the two displaced-strip measurements) takes 20 s. Therefore, the minute-rated measurements of $UV_G$, $UV_{Dif}$, and their corresponding $UV_{Dir}$ average on three cycles of measurements per minute. The UVMFR4 must be set up aligned with the meridian, where the accuracy in the positioning of the semicircular metallic strip is within 0.4°. The software controlling the instrument calculates both SZA and azimuth angle to set the strip correctly.

The instrument's sensor, radiation filters, and the associated electronic circuit are housed and sealed against moisture and rain (the moisture seal of the stepper motor can fail within a few months). The instrument works with internal temperature controlled around 41–42 °C for outdoor temperatures from −30 to +50 °C. Cosine correction is automatic for $UV_{Dir}$ with accuracy of 1% up to SZA = 80°, but no correction is attempted for $UV_G$ or $UV_{Dif}$. Typical uncertainties in these measurements are around 6–8% (Hülsen & Gröbner, 2007). Annual calibration at appropriate facilities is recommended to maintain such standards.

#### 2.2.2 *The Total Sky Imager*

The Total Sky Imager 440A (TSI, Yankee Environmental Systems, Inc., Turners Falls, MA, USA) measures cloud cover (cloudiness). It is composed of a digital camera facing down a rotating spherical mirror to photograph the reflected sky. A black strip is attached to the mirror in order to avoid direct reflection of sunbeams into the camera. Each snapshot results in a 24-bit color Joint Photographic Experts Group (JPEG) image with resolution of 352 × 288 pixels (101 kpixels). The software provided by the manufacturer and set up in a personal computer controls the TSI and processes captured images for cloudiness determination. Some of the software parameters must be adjusted by the operator in order to produce the best match between the sky observed by a trained operator and that determined by the equipment. Uncertainties in cloud cover measurements are greater than 10% in general (Silva & Souza-Echer, 2013).

#### 2.2.3 *The Ozone Monitoring Instrument (OMI)*

The Ozone Monitoring Instrument (OMI) flies on board the Aura satellite (Levelt et al., 2006; Taskanen et al., 2006). Launched in 2004 to orbit the Earth at Sun-synchronous polar orbits of 705 km, 98° inclination, and 13:45 ± 15 min equator-crossing time, the OMI has a two-dimensional charged coupled device (CCD) to measure UV/visible radiation (270–500 nm at 0.5 nm spectral resolution) from both DS radiation and radiation reflected from the Earth in swathes of 2600 km (115°) perpendicular to the satellite's flight direction. A pixel of the two-dimensional CCD corresponds to a ground grid whose size depends on the OMI cross track position (CTP). This parameter increases with the swath-angle from CTP = 0 for the null swath-angle of nadir (exact overpass measurements) and ground-grid of 13 km × 24 km (along × cross track, 312 $km^2$) to CTP = 59 for the swath-angle of 57° and ground-grid of 13 km × 150 km (1950 $km^2$). Since local boundary layer parameters such as site altitude, clouds, aerosols, and surface albedo can affect OMI measurements significantly, another important OMI parameter is the distance (Dist) between the coordinates of the site and the CTP ground-grid.

Differences between TOC measurements from ground-based instruments and OMI are around 2% (McPeters et al., 2008; Silva & Tomaz, 2012).

### 2.3. *Methods*

Spectral DS measurements were conducted in BH at the Laboratório de Luz Ultravioleta (LLUV, 19.92° S, 43.99° W, 910 m a.s.l.) from June 2009 (JUN09) to September 2010 (SEP10) (16 months)—when the noon solar zenith angle ($SZA_n$) ranges from 0° in summer (December, January, and February) to 43.4° in winter—using the calibrated radiometer UVMFR4 #566. The TSI #157 was set up beside the radiometer, also providing one sky image per minute. Measurements were conducted for air mass $m \leq 2$ (SZA < ≈ 60°).

Each of the four DS measurement wavelengths ($\lambda_1$ = 300 nm, $\lambda_2$ = 305.3 nm, $\lambda_3$ = 311.5 nm, $\lambda_4$ = 317.5 nm) can be applied to the fundamental atmospheric attenuation expression (or the Beer–

Bouguer–Lambert law) (Fleagle & Businger, 1980; McCartney, 1976)

$$I_{\lambda_i} = I_{o\lambda_i} e^{-\left(m_R \tau_{R\lambda_i} + m_{O_3} \tau_{O_3\lambda_i} + m_p \tau_{p\lambda_i}\right)}, i = 1, 2, 3, \text{ and } 4, \quad (2)$$

where $I_{\lambda_i}$ = spectral DS radiation in the atmosphere at $\lambda_i$; $I_{o\lambda_i}$ = spectral DS radiation at the top of the atmosphere at $\lambda_i$; $m_R = \sec(\mathrm{SZA})(1 - 0.0012(\sec^2(\mathrm{SZA}) - 1))$ is the relative optical air mass of the atmosphere for SZA $< \approx 75°$ (air mass $< \approx 4$) (Young, 1994); $m_{O_3} = \frac{R+h}{\sqrt{(R+h)^2 - (R+r)^2 \sin^2(\mathrm{SZA})}}$ is the relative optical air mass for ozone (meaning the ratio between the actual path of the solar radiation and the vertical line through the ozone layer) (Gao et al., 2001) with $R$ = 6371.229 km as the mean radius of the Earth, $r$ = site altitude (in km), and $h$ = 27.5 km as the ozone layer height for tropical sites (Kirchhoff & Guarnieri, 2002; NASA, 1976);

$m_p$ = the relative air mass for particles (aerosols and cloud droplets) in the atmosphere that is considered equal to $m_R$ for air mass $\leq 2$; $\tau_{R\lambda_i} = 0.008569\lambda_i^{-4}\left(1 + 0.0113\lambda_i^{-2} + 0.00013\lambda_i^{-4}\right)\frac{P}{P_o}$ is the atmospheric optical depth for air molecules, where $\lambda_i$ is in μm, $P_o$ = 101,325 Pa is the sea-level atmospheric pressure, and $P$ is the atmospheric pressure at the site (Teillet, 1990);

$\tau_{O_3\lambda_i} = (C_o(\lambda_i) + C_1(\lambda_i)(T_e - 273.15) + C_2(\lambda_i)(T_e - 273.15)^2)\mathrm{TOC}$ is the ozone optical depth, being TOC in cm, $C_o(\lambda_i)$ (in $\mathrm{cm}^{-1}$) the ozone absorption coefficient at normal temperature and pressure (NTP, 293.15 K and 1 atm), $C_1(\lambda_i)$ (in $\mathrm{cm}^{-1}\,\mathrm{K}^{-1}$) and $C_2(\lambda_i)$ (in $\mathrm{cm}^{-1}\,\mathrm{K}^{-2}$) the ozone absorption coefficients for temperature correction as a function of the effective atmospheric temperature $T_e$ (in K), which equals 229.6 K for the tropical atmosphere (Cervino et al., 1995); and $\tau_{p\lambda_i}$ = the particle optical depth corresponding to aerosols and cloud droplets in the atmosphere at $\lambda_i$.

Transforming Eq. (2) into

$$\ln(I_{\lambda_1}) = \ln(I_{o\lambda_1}) - m_R\tau_{R\lambda_1} - m_{O_3}\tau_{O_3\lambda_1} - m_p\tau_{p\lambda_1}, \quad (3)$$

$$\ln(I_{\lambda_2}) = \ln(I_{o\lambda_2}) - m_R\tau_{R\lambda_2} - m_{O_3}\tau_{O_3\lambda_2} - m_p\tau_{p\lambda_2}, \quad (4)$$

$$\ln(I_{\lambda_3}) = \ln(I_{o\lambda_3}) - m_R\tau_{R\lambda_3} - m_{O_3}\tau_{O_3\lambda_3} - m_p\tau_{p\lambda_3}, \quad (5)$$

$$\ln(I_{\lambda_4}) = \ln(I_{o\lambda_4}) - m_R\tau_{R\lambda_4} - m_{O_3}\tau_{O_3\lambda_4} - m_p\tau_{p\lambda_4}, \quad (6)$$

and making

$$(\ln(I_{\lambda_1}) - \ln(I_{\lambda_3})) - (\ln(I_{\lambda_2}) - \ln(I_{\lambda_4})), \quad (7)$$

to find TOC as (Dobson, 1931; Gao et al., 2001):

$$\mathrm{TOC} = \frac{\left[\ln\left(\frac{I_{o\lambda_1}}{I_{o\lambda_3}}\right) - \ln\left(\frac{I_{\lambda_1}}{I_{\lambda_3}}\right)\right] - \left[\ln\left(\frac{I_{o\lambda_2}}{I_{o\lambda_4}}\right) - \ln\left(\frac{I_{\lambda_2}}{I_{\lambda_4}}\right)\right] - m_R\left[\left(\beta_{R\lambda_1} - \beta_{R\lambda_3}\right) - \left(\beta_{R\lambda_2} - \beta_{R\lambda_4}\right)\right]\frac{N_A \mathrm{HP}}{V_{\mathrm{STP}} P_o}}{m_{O_3}\left[\left(\alpha_{O_3\lambda_1} - \alpha_{O_3\lambda_3}\right) - \left(\alpha_{O_3\lambda_2} - \alpha_{O_3\lambda_4}\right)\right]\frac{N_A}{V_{\mathrm{STP}}}}, \quad (8)$$

where $N_A = 6.022 \times 10^{23}$ air molecules/mol is Avogadro's number, $H = 8.4 \times 10^5$ cm the terrestrial atmosphere scale height, $V_{\mathrm{STP}}$ = 22,400 $\mathrm{cm}^3$ the volume of 1 mol of ideal gas at standard temperature and pressure (STP, 273.15 K and 1 atm) (Walker, 1977), $\alpha_{O_3\lambda_i}$(see Eq. (10)) and $\beta_{R\lambda_i}$(see Eq. (11)) the effective cross sections (in $\mathrm{cm}^2$) for absorption by ozone and attenuation by the atmosphere, respectively, at $\lambda_i$.

The uncertainty in TOC ($\sigma_{\mathrm{TOC}}$) was determined by the propagation analysis formula for uncertainties (ISO, 1995), considering $I_{\lambda_i}$($i$ = 1, 2, 3, and 4), $m_R$, $m_{O_3}$, and $P$ as the independent variables $x_j$ ($j$ = 1, 2, 3, 4, 5, 6, and 7) and their corresponding uncertainties $\sigma_j$:

$$\sigma_{\mathrm{TOC}} = \sqrt{\sum_{j=1}^{7} \left( \frac{\partial \mathrm{TOC}}{\partial x_j} \sigma_j \right)^2}. \qquad (9)$$

The four wavelengths of DS measurements centre filter bandwidths of 2.3–2.4 nm FWHM. Thus, all parameters depending on $\lambda_i$ must be turned into an effective value by weighing the parameter with the transmission function ($T_{\lambda_i}$) of the radiometer filters (Komhyr et al., 1993). For this, we define both (i) the effective ozone absorption cross section

$$\alpha_{O_3\lambda_i} = \frac{\sum_{j=1}^{N_{\lambda i}} T_{\lambda ij} \mathrm{CS}_{O_3\lambda ij}}{\sum_{j=1}^{N_{\lambda i}} T_{\lambda ij}}, \qquad (10)$$

where $\mathrm{CS}_{O_3\lambda_i} = \frac{C_o(\lambda_i)+C_1(\lambda_i)(T_e-273.15)+C_2(\lambda_i)(T_e-273.15)^2}{N_{\mathrm{A}}} V_{\mathrm{STP}}$ is the ozone absorption cross section (Cervino et al., 1995), and

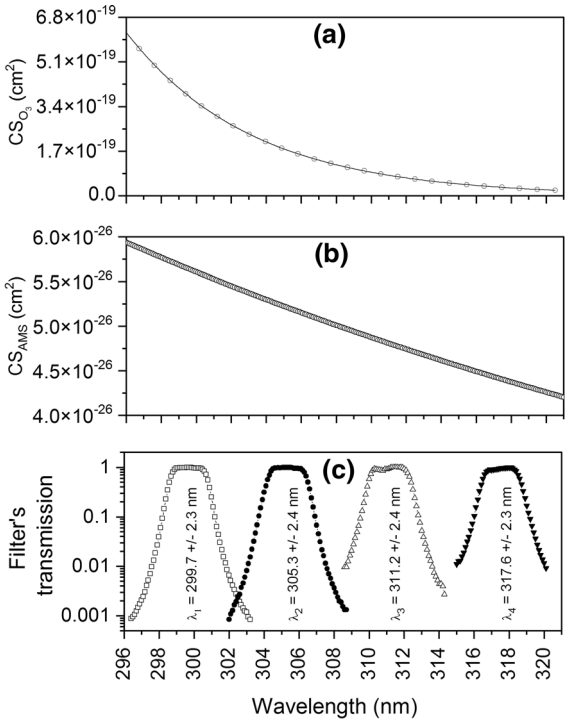


Figure 1

**a** The ozone absorption cross section. Data points have been fitted by the curve $\theta_{O_3} = (0.38 \pm 0.09)\mathrm{e}^{-(0.1384\pm0.0008)\lambda}$ with coefficient of determination $r^2$ = 0.999 and percent scattering SD% = 0.63% ($\mathrm{SD}\% = \mathrm{qmd} \cdot 100\%/(\mathrm{CS}_{O_3\,\max} - \mathrm{CS}_{O_3\,\min})$, where qmd is the quadratic mean difference between data points and fitting curve). **b** The atmospheric molecular scattering cross section. **c** The transmission function of the radiometer UVMFR4 #566 filters

(ii) the effective atmospheric molecular scattering cross section

$$\beta_{R\lambda_i} = \frac{\sum_{j=1}^{N_{\lambda i}} T_{\lambda ij} \mathrm{CS}_{\mathrm{AMS}\lambda ij}}{\sum_{j=1}^{N_{\lambda i}} T_{\lambda ij}}, \qquad (11)$$

where $\mathrm{CS}_{\mathrm{AMS}\lambda_i} = \frac{0.008569\lambda_i^{-4}\left(1+0.0113\lambda_i^{-2}+0.00013\lambda_i^{-4}\right)}{N_{\mathrm{A}}H} V_{\mathrm{STP}}$ is the atmospheric molecular scattering cross section (Teillet, 1990). Figure 1 shows $T_{\lambda_i}$ for the radiometer UVFMR4 #566 filters, $\mathrm{CS}_{\mathrm{AMS}\lambda_i}$, and $\mathrm{CS}_{O_3\lambda_i}$ for $T_e$ = 229.6 K.

From Eq. (7), the difference

$$-m_p\left[\left(\tau_{p\lambda_1} - \tau_{p\lambda_3}\right) - \left(\tau_{p\lambda_2} - \tau_{p\lambda_4}\right)\right], \qquad (12)$$

would come up in Eq. (8)'s numerator. Nonetheless, it has been neglected because the other differences in Eq. (8)'s numerator are much larger than it for the range of wavelengths ($\lambda_4 - \lambda_1$ = 17.5 nm) in this study (Dobson, 1931), as the dependence of the particle optical depth on radiation wavelength is usually low. Therefore, Eq. (8) indeed gives an approximation of the real value of TOC. However, neglecting that difference (Eq. (12)) is convenient, since we have no previous information regarding the particle optical depths.

The one-per-minute images yielded by TSI #157 gives a partial visual description of the sky and cloud cover during the measurement by the radiometer. In addition, the complete information for a given image is never obtained because the black strip attached to the TSI mirror blocks out the Sun and its immediate surrounding sky.

Regarding the sky cover during the radiometer measurements, three different scenarios are considered in this study. The first is the all-sky (AS) scenario with DS measurements occurring without any clouds blocking the Sun, but clouds are present in the sky. The investigation of the potential effect of such a scenario on TOC measurements is one of the goals here. Secondly, measurements occur with the Sun being blocked by some clouds (C) or, as a particular case of blocked Sun, a visible and identifiable aerosol plume (AP). And the third scenario is the cloud-free sky (CFS) that corresponds to a no-cloud sky period during which, naturally, the Sun is not blocked by any cloud, and therefore DS

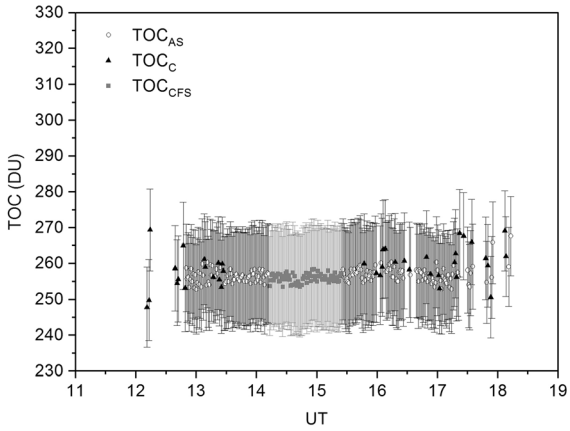


Figure 2
Total ozone column (TOC) measurements for all-sky scenarios ($TOC_{AS}$), cloud blocking the Sun ($TOC_C$), and cloud-free skies ($TOC_{CFS}$) on 13 March 2010 in Belo Horizonte. Bars are $1\sigma$ uncertainty

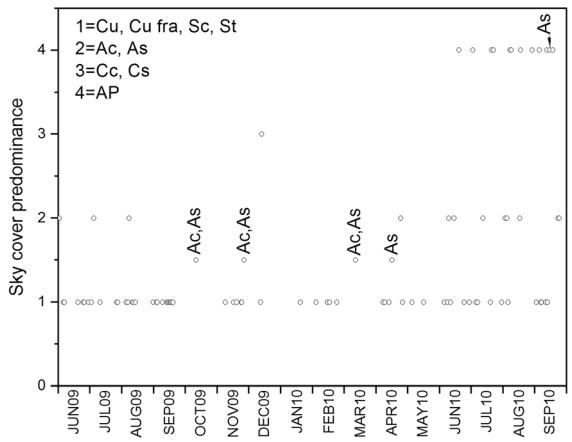


Figure 3
Sky cover predominance from June 2009 (JUN09) to September 2010 (SEP10) in Belo Horizonte during total ozone column measurements with clouds blocking the Sun. Note that sky-cover predominance on some days was a mix between groups 1 and 2, resulting in subgroup 1.5. In such cases, cloud genera of group 2 are shown as Ac (altocumulus) and As (altostratus). Cumulus (Cu), cumulus fractus (Cu Fra), stratocumulus (Sc), stratus (St), cirrocumulus (Cc), cirrostratus (Cs), and aerosol plume (AP) belong to other groups

measurements are free from the potential influence of clouds.

Linear-fitting comparisons of $TOC_{CFS}$ with $TOC_{OMI}$ measurements and measurements from the ground-based instrument MICROTOPS II #8461 are also provided.

## 3. Results

Figure 2 depicts TOC measurements for AS, C, and CFS scenarios on 13 March 2010, while Table 1 presents the corresponding daily averages ± 1 standard deviation (sd) as $\overline{TOC_{AS}}$, $\overline{TOC_C}$, and $\overline{TOC_{CFS}}$ in addition to the corresponding time periods to obtain the measurements.

Based on sky images from the TSI, the sky cover predominance is depicted in Fig. 3 in terms of the identification of cloud cover and AP for the 87 days corresponding to $TOC_C$ (or $TOC_{AP}$) values. Since the determination of the sky cover predominance was based solely on the analysis of TSI images, only four groups of cover (cloud or aerosol) have been selected (WMO, 1956): group 1 is low-altitude cumulus (Cu), cumulus fractus (Cu Fra), stratocumulus (Sc), and stratus (St) clouds; group 2 is middle-altitude altocumulus (Ac) and altostratus (As) clouds; group 3 is high-altitude cirrocumulus (Cc) and cirrostratus (Cs) clouds; and group 4 is for AP. In addition, there were also mixed scenarios where the sky was populated by similar shares of groups, resulting in subgroup representation by half-numbers, for

Table 1
*Daily averages ± 1 standard deviation (sd) as $\overline{TOC_{AS}}$, $\overline{TOC_C}$, and $\overline{TOC_{CFS}}$ on 13 March 2010 in Belo Horizonte and their corresponding measurement time periods ($\Delta T$)*

| | $\overline{TOC_{AS}}$ | $\overline{TOC_C}$ | $\overline{TOC_{CFS}}$ |
|---|---|---|---|
| Daily average ± 1 sd (DU) | 257 ± 2 | 259 ± 5 | 256 ± 1 |
| $\Delta T$ (min) | 173 | 40 | 72 |

DU stands for Dobson units (DU, 1 DU = 0.001 cm of TOC)

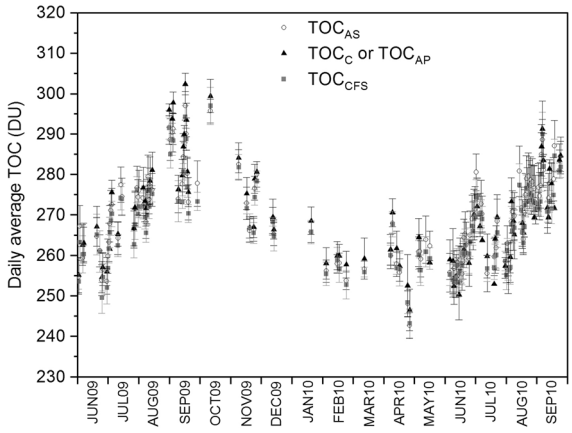


Figure 4
Daily averages of total ozone column (TOC) measurements for all-sky conditions ($TOC_{AS}$), cloud or aerosol plume blocking the Sun ($TOC_C$ or $TOC_{AP}$), and cloud-free skies ($TOC_{CFS}$) from June 2009 (JUN09) to September 2010 (SEP10) in Belo Horizonte. Bars are 1 standard deviation. Figure 3 shows when $TOC_C$ or $TOC_{AP}$ is to be considered

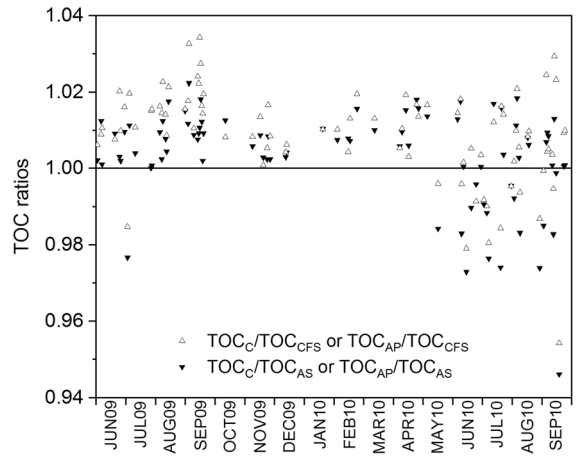


Figure 5
Ratios between daily averages of total ozone column measurements with cloud or aerosol plume blocking the Sun ($TOC_C$ or $TOC_{AP}$) and cloud-free skies ($TOC_{CFS}$) or all-sky conditions ($TOC_{AS}$) and $TOC_{CFS}$ from June 2009 (JUN09) to September 2010 (SEP10) in Belo Horizonte. Figure 3 shows when $TOC_C$ or $TOC_{AP}$ is to be considered

example 1.5, which derives from a sky with comparable contributions from groups 1 and 2.

The daily averages of $TOC_{AS}$, $TOC_C$, and $TOC_{CFS}$ from JUN09 to SEP10 are depicted in Fig. 4, with their variability represented by bars of 1 standard deviation. As shown by Silva (2013a), Usually, the diurnal variability in TOC measurements is small, being increased by the presence of clouds and aerosols. There were 138 days of measurements with AS and CFS scenarios for $TOC_{AS}$ and $TOC_{CFS}$, respectively, and 87 days with C scenarios for $TOC_C$. The minimum-to-maximum ranges were 243–297 Dobson units (DU) for both AS and CFS scenarios and 247–302 DU for C scenarios. Maximum and minimum values occurred by September–October (early spring) and April, respectively, as expected for a low-latitude Southern Hemisphere site (Silva, 2007; Whitten & Prasad, 1985).

However, daily time periods of measurements varied greatly. Thus, to make reliable comparisons of the variability in TOC measurements among the three AS, C, and CFS scenarios, one must obtain a time-independent parameter regarding TOC from days where the three scenarios occurred. Thus, Table 2 depicts—for the 75 days where the three scenarios AS, C, and CFS occurred daily with at least three TOC measurements each—the minimum ($T_{min}$), the average ($\overline{T}$), and the maximum ($T_{max}$) elapsed times to obtain the TOC measurements for each of the AS, C, and CFS scenarios, the three corresponding

Table 2

*For the 75 days where the three scenarios AS, C, and CFS occurred with at least three TOC measurements each in Belo Horizonte, the minimum ($T_{min}$), the average ($\overline{T}$), and the maximum ($T_{max}$) elapsed times to obtain daily TOC measurements for the AS, C, and CFS scenarios, the three corresponding average values of TOC for the three sets of 75 daily average values of TOC ($TOC_{75}$) ± 1 corresponding verage standard deviation ($sd_{75}$), and the variability rate ($sd_{75}/\overline{T}$)*

| Scenario | $T_{min}$ (min) | $\overline{T}$(min) | $T_{max}$ (min) | $\overline{TOC}_{75} \pm sd_{75}$(DU) | $sd_{75}/\overline{T}$(DU/min) |
|---|---|---|---|---|---|
| AS | 36 | 187 | 342 | 269 ± 4 | 0.02 |
| C | 3 | 25 | 114 | 271 ± 4 | 0.16 |
| CFS | 17 | 108 | 292 | 268 ± 3 | 0.03 |

DU stands for Dobson units (DU, 1 DU = 0.001 cm of TOC)

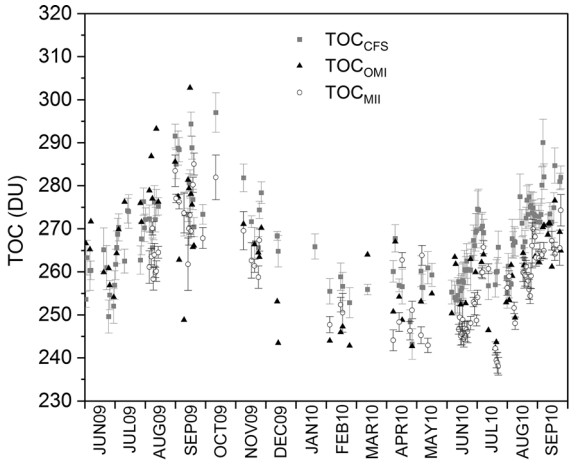


Figure 6
Total ozone column (TOC) measurements in Belo Horizonte from the UVMFR4 radiometer #566 for cloud-free skies (daily average $TOC_{CFS}$) and the Ozone Monitoring Instrument ($TOC_{OMI}$) from June 2009 (JUN09) to September 2010 (SEP10), and from the Microtops II #8461 (average $TOC_{MII}$) from August 2009 (AUG09) to SEP10

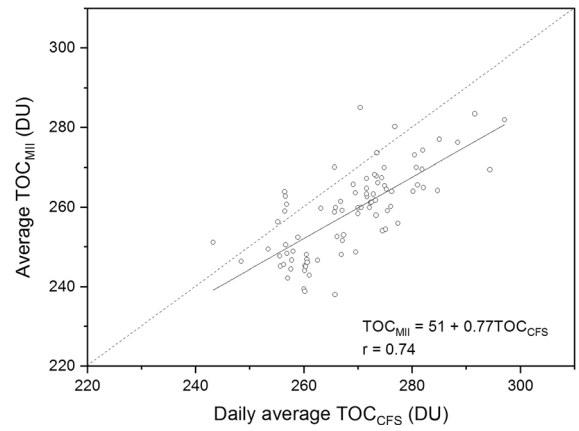


Figure 7
Linear fitting between total ozone column measurements from the handheld Microtops II #8461 (average $TOC_{MII}$) and the UVMFR4 #566 under cloud-free skies (daily average $TOC_{CFS}$) from June 2009 (JUN09) to September 2010 (SEP10) in Belo Horizonte

average values of TOC for the three sets of 75 daily average values of TOC ($TOC_{75}$) $\pm$ the corresponding average standard deviation ($\pm$ $sd_{75}$), and the TOC variability rate $sd_{75}/\overline{T}$ that represents the time-independent parameter.

The effects of clouds on TOC measurements are better depicted through the ratios $TOC_C/TOC_{CFS}$ and $TOC_C/TOC_{AS}$ as shown in Fig. 5 for those 75 days. The average $TOC_C/TOC_{CFS}$ equals 1.009 (0.9% increase in TOC measurement) with ratios from 0.954 (−4.6% reduction) to 1.034 (3.4% increase), while the average $TOC_C/TOC_{AS}$ equals 1.003 (0.3% increase) with ratios from 0.946 (−5.4% reduction) to 1.022 (2.2% increase). From the 87 days of C, 10 had $TOC_C/TOC_{CFS} < TOC_C/TOC_{AS}$, and some were, in fact, days with an aerosol plume blocking the Sun instead of a cloud, as indicated in Fig. 3. For those days, $TOC_C$ must be replaced with $TOC_{AP}$. Note also that 14 out of the 18 days with ratios $< 1$ were days within the dry period where AP scenarios are common, although not necessarily easy to identify.

Since there are ground-based and satellite TOC measurements from other works referring to BH, it is interesting to compare them with $TOC_{CFS}$, as CFS scenarios do not present the interference from clouds, although aerosol effects on the measurements can be present. Therefore, Fig. 6 shows 138 days of daily average $TOC_{CFS}$, 77 days of $TOC_{OMI}$ from OMI, and 84 days of average $TOC_{MII}$ from the handheld MICROTOPS II #8461 operated from August 2009 (AUG09) to SEP10 by Silva and Tomaz (2012). The average TOC from those three sets of data for the whole period were 268 $\pm$ 10 DU, 264 $\pm$ 12 DU, and 259 $\pm$ 11 DU, respectively. To deepen the comparison, linear fittings were applied to $TOC_{OMI}$ and $TOC_{MII}$ as a function of $TOC_{CFS}$. Figure 7 depicts $TOC_{CFS}$ vs. $TOC_{MII}$ and Table 3 shows the corresponding linear fitting parameters.

## 4. Discussion

Both detection and identification of clouds remotely can produce a misleading result. In fact, it is not trivial to detect the presence of some clouds or reasonably identify them by remote observation, since clouds such as As, for instance, can be taken erroneously as an AP and vice versa. It must be taken into account that what is seen in the sky remotely from the ground can even depend on the angle of visualization in relation to the Sun's position in the sky: the remote perception of a cloud is merely the detection of a radiation scattering phenomenon. Hence, there have been many situations where there has been significant doubt from the analysis of TSI

Table 3

*Parameters for the linear fitting ($Y = a + bX$) of $TOC_{CFS}$ vs $TOC_{MII}$ and $TOC_{CFS}$ vs. $TOC_{OMI}$ in Belo Horizonte. N and r refer to the number of data and the linear correlation, respectively, and SD% ($SD\% = qmd \cdot 100\%/(Y_{max} - Y_{min})$, where qmd is the quadratic mean difference between data points and fitting curve) is the percent scattering*

| Linear fitting | $a \pm \sigma$ (DU) | $b \pm \sigma$ | $N$ | $r$ | SD% (%) |
|---|---|---|---|---|---|
| $TOC_{CFS}$ vs. $TOC_{MII}$ | 51 ± 21 | 0.77 ± 0.08 | 84 | 0.74 | 14 |
| $TOC_{CFS}$ vs. $TOC_{OMI}$ | 74 ± 26 | 0.7 ± 0.1 | 77 | 0.64 | 18 |

DU stands for Dobson units (DU, 1 DU = 0.001 cm of TOC)

images regarding the precise identification of a stratus-genus cloud in relation to an AP. Such plumes identified from June 2010 (JUN10) to SEP10 (winter and early spring), as indicated in Fig. 3, were possibly mixed with As or other middle- and high-altitude stratus-genera in some days. The correct identification of C and AP scenarios is of utmost importance, as both can attenuate the solar radiation (Estupiñán et al., 1996). A study by Michelangeli et al. (1992) suggests that AP (or an aerosol layer) can also contribute to REEs.

In Table 1, the values of sd for $\overline{TOC_{AS}}$, $\overline{TOC_C}$, and $\overline{TOC_{CFS}}$ are much smaller than the uncertainties in each single TOC measurement in Fig. 2: the measurement uncertainty comes from Eq. (9) and represents $\approx$ 5% of TOC. Gao et al. (2001) found values of uncertainty of 2% in $TOC_{AS}$ considering a variability of 0.5% in DS measurements, while uncertainties of 8% (Hülsen & Gröbner, 2007) were assumed in DS measurements for this work. Nonetheless, from a statistical point of view, it can be said that $\overline{TOC_{AS}} = \overline{TOC_{CFS}}$ because of their 1–2 DU variability, while $\overline{TOC_C} \neq \overline{TOC_{CFS}}$ because of the variability of 1 DU in $\overline{TOC_{CFS}}$.

It seems that clouds cause such an effect. But how does it work? In the sky images produced by the TSI on 13 March 2010, there is a predominance of cloud genera Ac and As until 13:30 Universal Time (UT) and Sc and Cu Fra after 16:00 UT. Certainly, radiation attenuation played a role that day, but those cloud genera are also closely related to REE, yielding sudden (within a few tens of seconds) increases in the flux of radiation towards the ground from radiation scattering in clouds. Such sudden variations in the incidence of solar radiation could affect the values of $TOC_C$ because of the process used to obtain UVMFR4 measurements: $UV_G$, $UV_{Dif}$, and DS average three cycles of measurements within 1 min. Thus, regarding DS measurements, radiation attenuation by clouds within a few tens of seconds during the three cycles of $UV_G$, $UV_{Dif}$, and DS measurements would reduce the DS measurement, leading to a misleading perception, a false effect, of increased $TOC_C$. On the contrary, the sudden augmentation of radiation yielded by an REE would increase the value of the DS measurement, leading to a misleading perception of decreased $TOC_C$. Both effects could be responsible for the varying $TOC_C$ seen in Fig. 2 with 5 DU of standard deviation. Despite the outstanding characteristics of the TSI as an instrument, the black strip on its mirror represents a drawback that hinders this study, as the avoidance of direct reflection of sunbeams onto the TSI camera also unfortunately makes it impossible to exactly identify what (cloud or AP) and how (attenuation or REE) the Sun's radiation is blocked during UVMFR4 measurements. As a result, improving the current investigation into how clouds affect the values of $TOC_C$ is hampered for the time being. Nonetheless, Brogniez et al. (2005) and Houët and Brogniez (2004) in northern middle latitudes have observed results similar to those in Fig. 4, where in addition to larger values of $TOC_C$, larger variability in values was obtained.

The average ratio of 1.009 (0.9%) for $TOC_C/TOC_{CFS}$ and 1.003 (0.3%) for $TOC_C/TOC_{AS}$ from the daily ratios in Fig. 5 are an indication of cloud effects on DS measurements leading mainly to an increase in the value of $TOC_C$. Thus, radiation attenuation by clouds seems to be the preponderant factor here on average, as ratios tend to be $> 1$. On 13 March (Fig. 2), those ratios represented increases of 1–1.5% for mixed groups 1 and 2 of sky cover predominance.

For the 18 days with ratio $< 1$, 44% were caused by group 1 sky cover predominance, 17% by group 2, and 39% by group 4. However, more investigation is needed, especially regarding the more precise identification of what really blocks the Sun during DS measurements. This is a fundamental aspect regarding the identification of situations where attenuation or REEs can take place or even when an AP blocks the Sun instead of a cloud. To address this problem, a new imager has been developed by the author to make images of the sky without obstructions like those that occur with TSI's black strip blocking out the Sun and its immediate surroundings.

In the comparisons of $TOC_{CFS}$ vs $TOC_{MII}$ and $TOC_{CFS}$ vs $TOC_{OMI}$, whose linear fitting parameters are shown in Table 3, slope $b$ and intercept $a$ are all 95% confidence-level parameters, although the values of the linear correlations $r$ are just fair. The reason for the poorer $r$ is probably the difference among the data sets in terms of their particular meaning. While $TOC_{OMI}$ considers a 13:45 $\pm$ 15 min equator-crossing time OMI satellite measurement and $TOC_{MII}$ a ground-based DS measurement averaged over about 10 DS measurements as close as possible to the OMI overpass time (Silva & Tomaz, 2012), $TOC_{CFS}$ is a daily average obtained within a measurement time period $\Delta T$ that does not necessarily correspond to the same times as the other two data sets. Restricting the satellite parameter Dist to impose only the use of satellite data corresponding to the site's territorial area leads to quite a superior value of $r = 0.91$ for $TOC_{MII}$ vs $TOC_{OMI}$, as shown by Silva and Tomaz (2012) for the same site.

Silva (2013a) and Silva and Tomaz (2012) have shown that the variability in TOC depends significantly on cloudiness, as the sd can be $< 1\%$ of TOC for CFS scenarios and $< 4\%$ of TOC for AS ones. The average $TOC_C/TOC_{CFS}$ larger than the average $TOC_C/TOC_{AS}$ also implies that the very presence of clouds is enough to affect DS measurements, although no cloud had blocked the Sun for CFS or AS scenarios. Nonetheless, a true verification of the sky cover predominance effect on TOC measurements must naturally be time-independent. Thus, considering just the 75 days where each of the three scenarios AS, C, and CFS occurred daily with at least three TOC measurements, one calculates the $sd_{75}/\overline{T}$ ratio shown in Table 2. As a TOC variability rate, this ratio is time-independent, and for C scenarios it is over five times larger than the ratio for the other two scenarios, implying a higher variability caused by clouds in the values of TOC measurements through attenuation and REE.

## 5. Conclusions

TOC measurements were drawn from DS measurements by a UVMFR4 radiometer for 16 months in a tropical site. Although uncertainties of about 5% were found in TOC measurements, their variability was generally smaller for all-sky conditions without clouds blocking the Sun (AS) and cloud-free skies (CFS) scenarios. The presence of clouds seems to affect not only the value of TOC, but also the variability of a set of measurements, especially if clouds block the Sun (C scenarios). Thus, the averages of $TOC_C/TOC_{CFS} = 1.009$ (0.9%), ranging from 0.954 ($-4.6\%$) to 1.034 (3.4%), and $TOC_C/TOC_{AS} = 1.003$ (0.3%), ranging from 0.946 ($-5.4\%$) to 1.022 (2.2%), indicate an average increase of 0.9% and 0.3% in the values of TOC measurements yielded by clouds in relation to CFS and AS scenarios, respectively, while the time-independent variability in TOC (the $sd_{75}/\overline{T}$ ratio) was over five times larger for C scenarios than CFS scenarios on average. Thus, clouds affect TOC measurements with respect to both the measured values and, in particular, their variability.

Since the average $TOC_C/TOC_{CFS}$ was larger than 1, it seems that radiation attenuation by clouds is the main factor responsible for the apparent increase in TOC. However, REEs can play an important role here, as 14 out of 18 $TOC_C/TOC_{CFS}$ ratios $< 1$ were under AP scenarios, which sometimes come mixed with stratus-genera clouds, leading to the conclusion that the REE potential effects on TOC measurements deserve more investigation. Unfortunately, the determination of the real effect during DS measurements is not achievable for the time being due to the image partial blockage represented by TSI's black strip. However, the development of a new imager producing images without any blockage (like the black strip on the TSI mirror) of the sky, thereby

showing the Sun disc and its immediate surroundings, will enable the improvement of such an investigation.

**Author Contributions** The author is the only contributor.

### *Funding*

I thank the Conselho Nacional de Desenvolvimento Científico e Tecnológico (CNPq) and the Fundação de Amparo à Pesquisa do Estado de Minas Gerais (FAPEMIG).

### *Availability of Data and Material*

Data are available from the author upon request.

### *Code Availability*

Not applicable.

**Declarations**

**Conflict of interest** The author declares no conflict or competing interest.

**Ethics approval** Not applicable.

**Consent to participate** Not applicable.

**Consent for publication** Pure and Applied Geophysics is allowed to publish it.

**Publisher's Note** Springer Nature remains neutral with regard to jurisdictional claims in published maps and institutional affiliations.

## References

Bais, A. F., McKenzie, R. L., Bernhard, G., Aucamp, P. J., Ilyas, M., Madronich, S., & Tourpali, K. (2015). Ozone depletion and climate change: impacts on UV radiation. *Photochemical and Photobiological Sciences, 14*, 19–52. https://doi.org/10.1039/c4pp90032d

Brogniez, C., Houët, M., Siani, A. M., Weihs, P., Allaart, M., Lenoble, J., Cabot, T., Casiniére, A., & Kyrö, E. (2005). Ozone column retrieval from solar UV measurements at ground level: Effects of clouds and results from six European sites. *Journal of Geophysical Research, 110*, D24202. https://doi.org/10.1029/2005JD005992

Calbó, J., Pagès, D., & González, J.-A. (2005). Empirical studies of cloud effects on UV radiation: A review. *Reviews of Geophysics, 43*, RG2002. https://doi.org/10.1029/2004RG000155

Cervino, M., Canossi, I., Guzzi, R., & Torricela, F. (1995). Temperature-dependent ozone transmission in a mono-layer atmospheric model. *International Journal of Remote Sensing, 16*, 375–381.

Chiu, J. C., Marshak, A., Knyazikhin, Y., Pilewski, P., & Wiscombe, W. J. (2009). Physical interpretation of the spectral radiative signature in the transition zone between cloud-free and cloudy regions. *Atmospheric Chemistry and Physics, 9*, 1419–1430. https://doi.org/10.5194/acp-9-1419-2009

Dobson, G. M. B. (1931). A photoelectric spectrophotometer for measuring the amount of atmospheric ozone. *Proceedings of the Physical Society, 43*, 324–328.

Estupiñán, J. G., Raman, S., Crescenti, G. H., Streicher, J. J., & Barnard, W. F. (1996). Effects of clouds and haze on UV-B radiation. *Journal of Geophysical Research, 101*, 16807–16816.

Fleagle, R. G., & Businger, J. A. (1980). *An introduction to atmospheric physics*. Academic Press.

Gao, W., Slusser, J., Gibson, J., Scott, G., Bigelow, D., Kerr, J., & McArthur, B. (2001). Direct-sun column ozone retrieval by the ultraviolet multifilter rotating shadow-band radiometer and comparison with those from Brewer and Dobson spectrophotometers. *Applied Optics, 40*, 3149–3155.

Harrison, L., Michalsky, J., & Berndt, J. (1994). Automated multifilter rotating shadow-band radiometer: An instrument for optical depth and radiation measurements. *Applied Optics, 33*, 5118–5125.

Houët, M., & Brogniez, C. (2004). Ozone column retrieval from solar UV irradiance measurements at ground level: Sensitivity tests and uncertainty estimation. *Journal of Geophysical Research, 109*, D15302. https://doi.org/10.1029/2004JD004703

Hülsen, G., & Gröbner, J. (2007). Characterization and calibration of ultraviolet broadband radiometers measuring erythemally weighted irradiance. *Applied Optics, 46*, 5877–5886.

IBGE. (2021, May 31). *Cidades*. Retrieved May 31 2021, from https://cidades.ibge.gov.br

ISO. (1995). *Guide to the expression of uncertainty in measurement*. International Standard Organization.

Kirchhoff, V. W. J. H., & Guarnieri, F. L. (2002). Missing ozone at high altitude: Comparison of in situ and satellite data. *Journal of Geophysical Research, 107*, 4109. https://doi.org/10.1029/2001JD000810

Komhyr, W. D., Mateer, C. L., & Hudson, R. D. (1993). Effective Bass-Paur 1985 ozone absorption coefficients for use with Dobson ozone spectrophotometers. *Journal of Geophysical Research, 98*, 20451–20465.

Koren, I., Remer, L. A., Kaufman, Y. J., Rudich, Y., & Martins, J. V. (2007). On the twilight zone between clouds and aerosols. *Geophysical Research Letters, 34*, L08805. https://doi.org/10.1029/2007GL029253

Lautenschlager, S. H., Wulf, H. C., & Pittelkow, M. R. (2007). Photoprotection. *The Lancet, 370*, 528–537. https://doi.org/10.1016/S0140-6736(07)60638-2

Levelt, P. F., van den Oord, G. H. J., Dobber, M. R., Mälkki, A., Visser, H., de Vries, J., Stammes, P., Lundell, J. O. V., & Saari, H. (2006). The ozone monitoring instrument. *IEEE Transactions*

*on Geoscience and Remote Sensing, 44*, 1093–1101. https://doi.org/10.1109/TGRS.2006.872333

McCartney, E. J. (1976). *Optics of the Atmosphere*. John Wiley & Sons.

McPeters, R., Kroon, M., Labow, G., Brinksma, E., Balis, D., Petropavlovskikh, I., Veefkind, J. P., Bhartia, P. K., & Levelt, P. F. (2008). Validation of the aura ozone monitoring instrument total column ozone product. *Journal of Geophysical Research, 113*, D15S14. https://doi.org/10.1029/2007JD008802

Michelangeli, D. V., Allen, M., Yung, Y. L., Shia, R.-L., Crisp, D., & Eluszkiewicz, J. (1992). Enhancement of atmospheric radition by an aerosol layer. *Journal of Geophysical Research, 97*, 865–874.

NASA. (1976). *US standard atmosphere, 1976*. Government Printing Office.

Parisi, A. V., & Dows, N. (2004). Variation of the enhanced biologically damaging solar UV due to clouds. *Photochemical & Photobiological Sciences, 3*, 643–647.

Silva, A. A. (2007). A quarter century of TOMS total column ozone measurements over Brazil. *Journal of Atmospheric and Solar-Terrestrial Physics, 69*, 1447–1458. https://doi.org/10.1016/J.JASTP.2007.05.006

Silva, A. A. (2011). Local cloud cover, ground-based and satellite measurements of erythemal dose rate for an urban, tropical site in Southern Hemisphere. *Journal of Atmospheric and Solar-Terrestrial Physics, 73*, 2474–2481. https://doi.org/10.1016/j.jastp.2011.09.002

Silva, A. A. (2013a). Ground-based total ozone column measurements and their diurnal variability. *Journal of Geophysical Research, 118*, 7344–7349. https://doi.org/10.1002/jgrd.50568

Silva, A. A. (2013b). Erythemal dose rate under noon overcast skies. *Photochemical & Photobiological Sciences, 12*, 777–786. https://doi.org/10.1039/C2PP25330E

Silva, A. A., & Souza-Echer, M. P. (2013). Ground-based measurements of local cloud cover. *Meteorology and Atmospheric Physics, 120*, 201–212. https://doi.org/10.1007/s00703-013-0245-9

Silva, A. A., & Tomaz, L. M. (2012). Total ozone column measurements for an urban, tropical site in the Southern Hemisphere with a Microtops II. *Journal of Atmospheric and Solar-Terrestrial Physics, 77*, 161–166. https://doi.org/10.1016/j.jastp.2011.12.014

Silva, A. A., Yamamoto, A. L. C., & Corrêa, M. P. (2019). Daily maximum erythemal dose rates in the tropics. *Photochemistry and Photobiology, 95*, 886–894. https://doi.org/10.1111/php.13054

Tanskanen, A., Krotkov, N. A., Herman, J. R., & Arola, A. (2006). Surface ultraviolet irradiance from OMI. *IEEE Transactions on Geoscience and Remote Sensing, 44*, 1267–1271. https://doi.org/10.1109/TGRS.2005.862203

Teillet, P. M. (1990). Rayleigh optical depth comparisons from various sources. *Applied Optics, 29*, 1897–1900.

Walker, J. C. G. (1977). *Evolution of the atmosphere*. Macmillan Publishing Co., Inc.

Whitten, R. C., & Prasad, S. S. (1985). *Ozone in the free atmosphere*. Van Nostrand Reinhold Company.

WMO. (1956). *International Cloud Atlas*. World Meteorological Organization.

Young, A. T. (1994). Air mass and refraction. *Applied Optics, 33*, 1108–1110.

(Received June 29, 2021, revised December 6, 2021, accepted December 7, 2021, Published online January 22, 2022)